Chapter 1 Introduction

Part I Surface structure:

1-1 Why is Ultrahigh Vacuum Used ?

In order to study atomically clean surface, we must work under so-called ultrahigh vacuum (UHV) conditions. In practice, one usually wants to study a surface without worrying about contamination from ambient gases. Thus, keeping the experimental environment clean is the most important key point in the study of surface science. As the following, rough calculation of the flux F of molecules striking the surface of unit area at an ambient pressure P is given by

$$F = \frac{N_A P}{\sqrt{2\pi MRT}} \tag{1-1}$$

where N_A is Avogadro's number, M is the average molar weight of the gaseous species, R is the gas constant, T is the temperature. Thus, the formula above can be easily transformed as the following

$$F(atoms/cm^2 \cdot \sec) = 3.51 \times 10^{22} \frac{P(Torr)}{\sqrt{M(g/mole)T}} \tag{1-2}$$

When we substitute $P = 10^{-9}$ $Torr$ and using the values $M = 28$ $g/mole$ and $T = 300$ K, we obtain $F \approx 10^{11}$ $atoms/cm^2 \cdot \sec$. On the other hand, each atom or molecular encounters an attractive potential that will bind it to the surface which is so-called "absorption". Thus, the absorbed surface concentration σ (in $molecules/cm^2$) of molecules on an initially clean surface is given by the product of the incident flux F and the residence time τ :

$$\sigma = F \cdot \tau \tag{1-3}$$

Assuming that each incident gas molecular sticks on the Pt(111) surface ($\approx 3 \times 10^{14}$ $atoms/cm^2$) and has a sticking coefficient of unity, it may take the order of hour before a clean surface is covered the molecules completely. This time usually needed to perform experiments on clean surfaces. That's the main reason why is UHV so necessary.

1-2 Surface Structure of Pt(111) substrate

The structure of Pt(111) surface is the close-packed surface of face-centered cubic (fcc) crystal. The schematic figures in real space and reciprocal space are shown in the following.

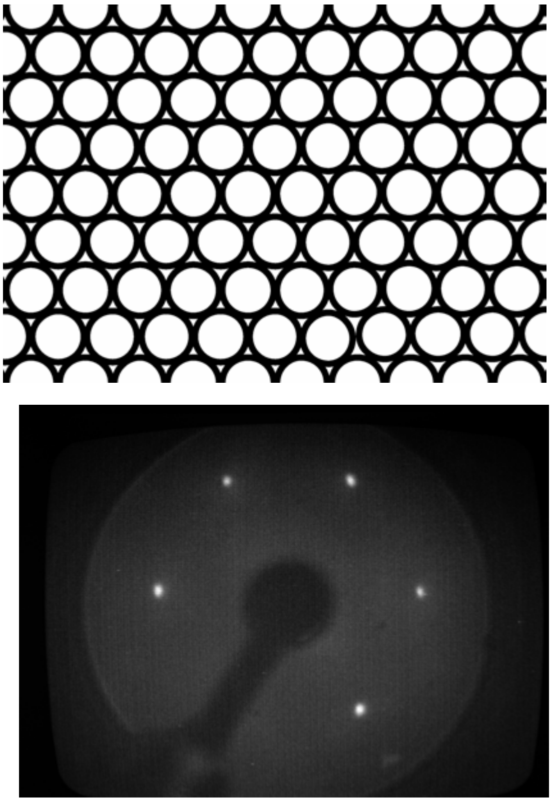

(a) Real lattice

(b) Reciprocal lattice

Fig. 1-1 (a) Scheme diagram of Pt(111) surface in real space, and (b) LEED pattern of clean Pt(111) in reciprocal space. The picture in (b) was captured by the incident electron beam energy of 120 eV.

There are two conventions in common use to define the relationship between the adsorbate and substrate surface, i.e.—the matrix notation[1] and the Wood notation.[2]

The most general notation for relating the primitive translation vectors of the substrate lattice and those of the surface is the matrix notation by Park and Madden. A practical surface may have periodic translations different from those predicted from the bulk, i.e., a different unit cell with unit-cell vectors $\vec{a}^*$ and $\vec{b}^*$ that differ from those, $\vec{a}$ and $\vec{b}$, obtained from the bulk projection. Then the surface unit-cell vectors $\vec{a}^*$ and $\vec{b}^*$ can be expressed as

$$\begin{aligned} \vec{a}^* &= m_{11}\vec{a} + m_{12}\vec{b} \\ \vec{b}^* &= m_{21}\vec{a} + m_{22}\vec{b} \end{aligned} \tag{1-4}$$

where the coefficients m_{11}, m_{12}, m_{21}, and m_{22} define a matrix

$$M = \begin{pmatrix} m_{11} & m_{12} \\ m_{21} & m_{22} \end{pmatrix} \tag{1-5}$$

The Wood notation uses the ratios of the lengths of the primitive vectors for the substrate and the surface vector, together with the angle through which one lattice must be rotated to align the two pairs of vectors. If the lattice vectors are related by

$$|a^*| = m|a| \quad \text{and} \quad |b^*| = n|b| \tag{1-6}$$

and the angle between them is ϕ, then the structure of the (hkl) surface is referred to as

$$(hkl)(m \times n)R\phi^\circ \tag{1-7}$$

If no rotation of the lattices are required to align their lattice vectors ($\phi = 0^\circ$) then the suffix specifying the ϕ angle can be dropped.

For some examples, an arrangement of the surface atoms identical to that in the Pt (111) bulk unit cell which is called the substrate structure and is designated (1×1) corresponding to the $\begin{pmatrix} 1 & 0 \\ 0 & 1 \end{pmatrix}$ matrix notation. The picture is schematic in Fig. 1-2a. If the unit cell of the surface structure is twice as large as the underlying bulk unit cell, it is designated (2×2), corresponding to the $\begin{pmatrix} 2 & 0 \\ 0 & 2 \end{pmatrix}$ matrix notation. The structure is schematic in Fig. 1-2b. Another well-known superstructure of $\left(\sqrt{3} \times \sqrt{3}\right)R30^\circ$ corresponding to the $\begin{pmatrix} 1 & -1 \\ 1 & 2 \end{pmatrix}$ matrix notation may arise. The superstructure is shown in Fig. 1-2c. The angle given after the notation and the letter R indicate the orientation of the surface structure, which is rotated with respect to the original substrate unit cell.

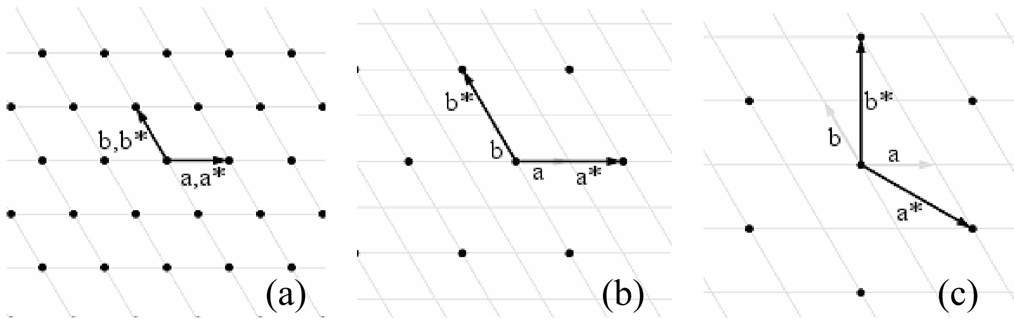

Fig. 1-2 The common surface structures of the thin film. (a) p(1×1), (b) p(2×2), and (c) $\left(\sqrt{3} \times \sqrt{3}\right)R30^\circ$ structures. The light-gray meshes are the unit mesh of the substrate structure. The black spots are the adsorbed atoms. The light-gray arrows are the primitive vectors $\vec{a}$ and $\vec{b}$, and the black arrows are the surface unit-cell $\vec{a}^*$ and $\vec{b}^*$.

1-3 Surface Energies and Growth Modes at Metal Surfaces

In general, the three markedly different modes of film growth can be distinguished below:

Ⅰ. *Frank-van der Merwe growth mode (FM mode)*

The growth mode is also called *layer-by-layer* growth, which the deposited metal may form with the second layer beginning only after the first layer is complete. The interaction between substrate and layer atoms is stronger than that between neighboring layer atoms. It is shown schematically in Fig. 1-3a.

II. *Stranski-Krastanov growth mode (SK mode)*

The subsequent thin film growth after the first complete layer continues instead with the formation 3-dimentional (3-D) islands. A certain lattice mismatch between substrate and deposited film may not be able to be continued into the bulk of the epitaxial crystal. Alternatively, the symmetry or orientation of the overlayers with respect to substrate might be responsible for producing this mode. The schematic diagram see in Fig. 1-3b.

III. *Volmer-Weber growth mode (VW mode)*

The growth is fully depending on the formation of 3-D islands form from the very beginning of the metal deposition. In contrast with the *FM* mode, the interaction between neighboring film atoms exceeds the overlayer substrate interaction. An island deposit always means a multilayer conglomerate of adsorbed atoms. Fig. 1-3c

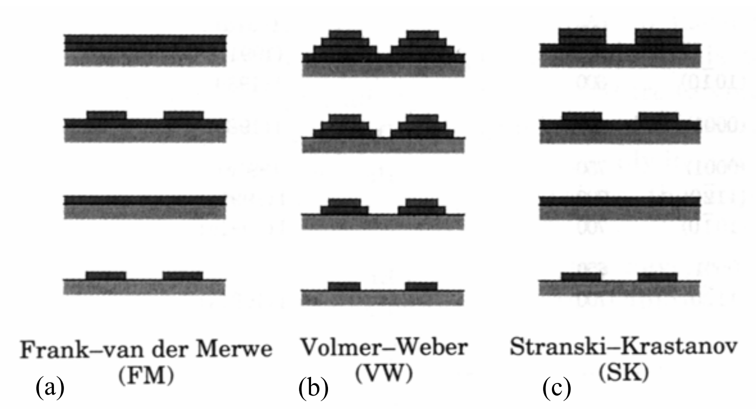

Fig. 1-3 Classification of epitaxial growth modes.

However, the occurrence of the various growth mode can be made in terms of surface or interface energy γ, i.e., the characteristic free energy (per unit area) to create an additional piece of surface or interface. Bauer was the first to note that the growth modes of thin films can be considered as a wetting problem, governed by $\Delta\gamma = \gamma_f + \gamma_i - \gamma_s$, where γ_s, γ_f, and γ_i are the surface energy of the substrate, the growing film and the interface energy, respectively. If the film grows near equilibrium, it wets the surface and therefore starts growing by a monolayer if $\Delta\gamma < 0$; on the other hand, it starts growing by 3-D nuclei when $\Delta\gamma > 0$. Because of the strain energies, one must be included in the surface energies of layer-grown film. However, metallic interface energies are one order of magnitude lower than surface energies and hard to measure, the growth mode is governed essentially by surface energies. Some selected data of our research metals are reported in the following table 1-1

TABLE 1-1[3]

	Selected adsorbate metals			
	Ag	Ni	Co	Pt
$\gamma(J/m^2)$	1.25	2.45	2.55	2.55

On the other hand, the growth process can be accurately followed using diffraction since the reflected signal is sensitive to surface roughness. The specular beam is the central diffraction rod and labeled as the (h, k)=(0, 0) rod. Maximum sensitivity to surface roughness is obtained for points on this rod exactly in between two bulk peaks. In this case the signal from one layer is exactly out-of-phase (destructive interference) with that of the underlying one.

The atoms do not reach a step edge, but encounter other deposited atoms with which they form two-dimensional island (2D island nucleation). Initially the islands grow and the diffracted intensity decreases, because of the destructive interference of the signal from the islands with that of the lower lying layer (Fig. 1-4a). At 0.5 ML

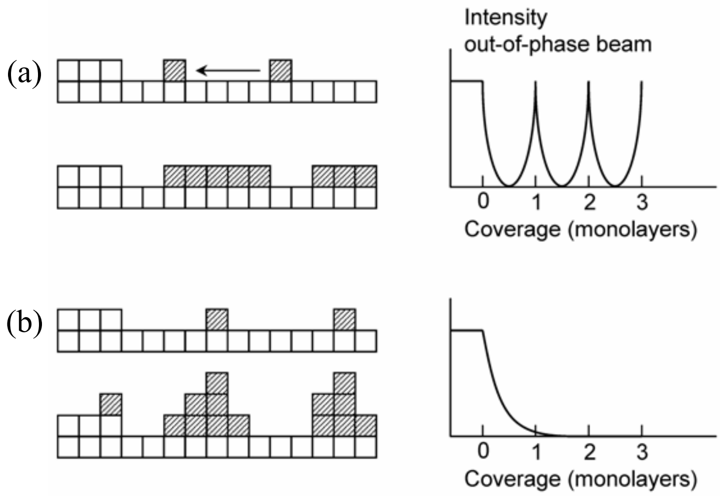

Fig. 1-4 A schematic diagram of the growth (a) ideal layer-by-layer and (b) rough island growth.[4]

coverage, the diffracted intensity becomes zero. Upon further deposition, the islands start to coalesce and the intensity increases again. If the layer would perfectly close itself before islands are formed on the next level, the intensity would reach the starting level and one speaks of ideal layer-by-layer growth. One would observe an oscillatory intensity with constant amplitude and with a period corresponding to the growth of one monolayer. In practice, this ideal behavior does not occur and damped oscillations are found instead. In other words, the atoms are largely immobile and the surface becomes rough quickly (Fig. 1-4b). During this rough growth, no oscillations are observed and the signal decays rapidly.

1-4 Lattice Misfit (Lattice Mismatch)

A second important parameter determining epitaxial growth is the lattice misfit, η, defined in a one-dimensional model by

$$\eta = \frac{b' - a'}{a'} \qquad (1\text{-}8)$$

where b' and a' are the lattice parameters of film and substrate, respectively. If the contacting lattice planes of both crystals show the same two-dimensional symmetry, the definition applies too for interfaces. Misfits for selected magnetic on homosymmetric epitaxial substrates are given in the following table 1-2.

TABLE 1-2

Substrate Metal		η (%) for different film metals		
		Ni	Co	Ag
	$\boldsymbol{a'}$	$\boldsymbol{b'}$=3.524	$\boldsymbol{b'}$=3.550	$\boldsymbol{b'}$=4.086
Ni	3.524	0	0.7	15.9
Co	3.550	−0.7	0	15.1
Pt	3.924	−10.2	−9.5	4.1
Ag	4.086	−13.8	−13.1	0

For interfaces with large lattice mismatch may lead to epitaxial pseudomophic overlayers which adopt the substrate surface symmetry and lattice constants. However, the considerable strain still exists in the first layers of the film. With increasing film thickness the strain will exceed the interface bond energy and the overlayer will relax to its bulk lattice constants, which may lead to a large number of near interface dislocation.[5] The dislocation coming from the misfit of the overlayer and the substrate might induced a Moiré pattern.[6,7] A perfect Moiré pattern can only be observed for two layers that have a different lattice constant and are coherent, i.e., have no defects. For instance, a top-view representation of a hard sphere model of the atomic arrangement with about 10% lattice mismatch between Pt and Ni is given in Fig. 1-5a.

(a)

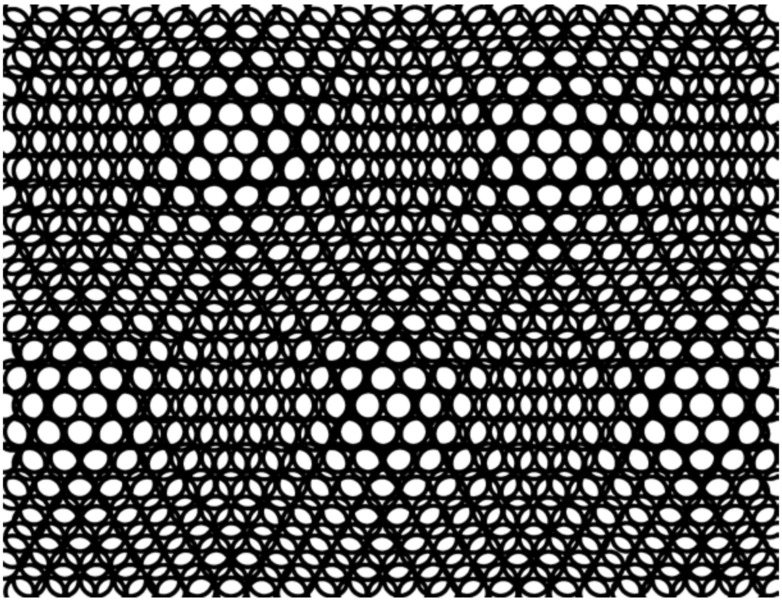

(b)

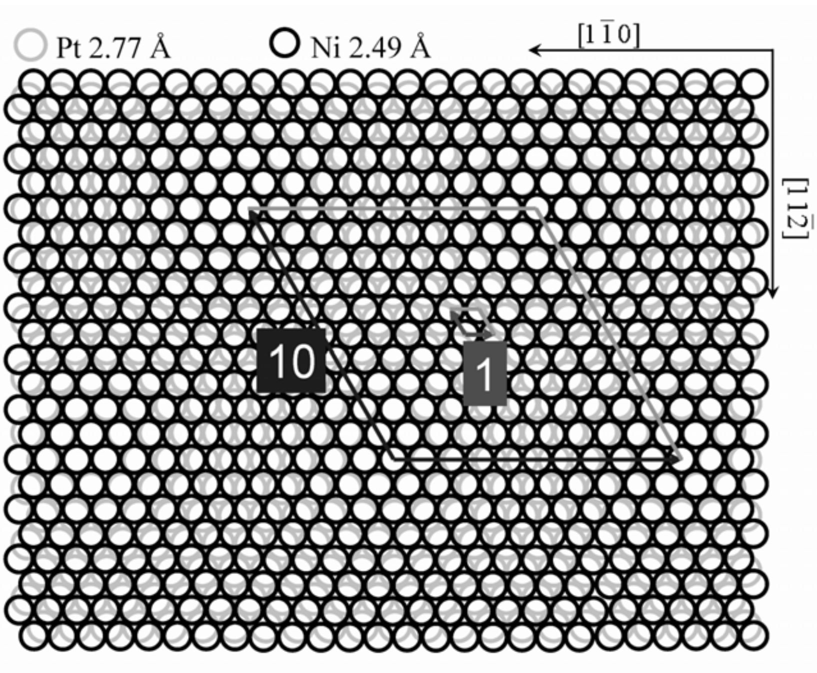

Fig. 1-5 (a) A top view of the interface of two unrotated hexagonal closest packed lattices with a 10% lattice misfit showing the Moiré pattern. (b) Periodic lattice distortions with a supermesh of 10 Ni atomic distances calculated from the Moiré expression without rotation.

The Moiré pattern shown in the top view assumes that there is no rotation between the epilayer and the substrate. The average size of the structures can be predicted using the Moiré equation as the following

$$D = \frac{a_1 a_2}{\left| a_1 - a_2 \right|} \tag{1-9}$$

where D is the length of the supermesh, a_1 and a_2 are the lattice constants of the epilayer and the substrate. In other words, on-top atoms at the interface show us the misfit can be calculated from the cell size as usual for a Moiré pattern of $n \times n$ surface atoms on $(n-1) \times (n-1)$ substrate atoms. In consequence, periodic lattice distortion with a supermesh of 10 Ni atomic distances is given in Fig. 1-5b. The periodic lattice distortions in real space correlated to lattice mismatch conditions had been postulated by scanning tunneling microscopy (STM) measurements.[7-9]

Moreover, the appearance of a Moiré structure in LEED can in principle be caused by two different scattering mechanisms.

1. Multiple scattering between substrate and film in the interface region.
2. Scattering at an undulated film that is locked in at nearly commensurate substrate positions forms a phase grating for the scattered electrons.

Part II Surface magnetism:

1-5 Magnetization of Ferromagnetic materials

Interest in surface and thin film magnetism is driven both by scientific curiosity and technical applications. The magnetism at the surface or in an ultrathin film is very different from the bulk magnetism of the same material. This is a result of the altered coordination and symmetry at the surface, leading to Néel surface anisotropy, and in some cases to strong magnetoelastic interactions. These effects are most clearly manifest in the appearance of perpendicular magnetic anisotropy in many thin film systems. A variety of polarized electron techniques are capable of revealing the preferred direction of magnetization in a thin film or at a surface. This is revealed in the shape of the $M-H$ (or $\theta_k - H$ or polarization vs. H) loops for different field orientation.

When a magnetic field is applied to a ferromagnetic specimen, the magnetization may vary from zero to the saturation value. The general appearance is shown in Fig. 1-6.

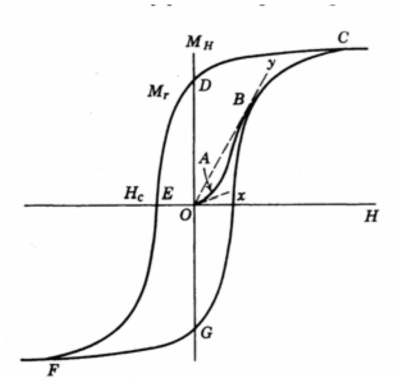

Fig. 1-6 Magnetization curve (OABC) and hysteresis loop (CDEFGC) of a typical ferromagnetic material.

The material is initially in a demagnetized state, indicated by *O*. When a field is applied, the magnetization M_H increases until the saturation value is reached. This behavior is indicated by the curve *OABC*. By performing the sequence of operations of reducing the field to zero, increasing it in the reverse direction, decreasing it to zero, and then increasing it to the original value, the curve *CDEFGC*, known as a hysteresis curve or loop, is obtained. When the field *H* is decreased to zero from point *C* on the initial magnetization curve the magnetization does not return to zero but instead decreases to the value M_r known as the *remanent magnetization* or *remanence*. The macroscopic magnetization of the material can be decreased to zero only by overcoming the effects of the pinning of the domain walls through the application of a magnetic field in the opposite direction. Thus, the reverse field needed to restore *M* to zero is called the *coercive field* or *coercivity*.

1-6 Magnetic anisotropies in ultrathin films

When a physical property of a material is a function of direction, that property is said to exhibit anisotropy. The preference for the magnetization to lie in a particular direction in a sample is called magnetic anisotropy. One of the most remarkable properties of ultrathin film magnetic films is given by their unusual magnetic anisotropies. Therefore, the following lists are the common discussions of magnetic film phenomena with magnetic anisotropies. The anisotropy is given by the contribution to the free energy of the crystalline film which depends on the direction of the magnetization. One defines the direction by the polar angle θ with respect to the sample normal and azimuth angle φ with respect to some low symmetric direction in the plane. In general, with a homogenous magnetization approximation, one can consider the following anisotropy contributions:

(i) Magnetostatic anisotropy (shape anisotropy)
(ii) Magnetocrystalline anisotropy
(iii) Magnetoelastic anisotropy (strain anisotropy)
(iv) Magnetic surface anisotropy

Néel (1954) was the first to note that the dramatic break of local magnetic symmetry in a surface must result in strong surface-type anisotropies. In a phenomenological sense, they are a magnetic contribution to the free energy (interface) energy of the crystal. If there is an anisotropy K_s localized at the surface that differs from that of the bulk, the effective anisotropy energy density measured for a thin film of thickness *d*, may be described as the following [10]

$$K^{eff} = \frac{1}{d}\int_0^d \left(K^v + K^s\delta(z)\right)dz \qquad (1\text{-}10)$$

where K^v is the bulk anisotropy energy density operating uniformly throughout the film and K^s is an energy per unit area localized at the surface (z = 0) by the Dirac delta function $\delta(z)$. Thus the effective anisotropy energy density can be expressed by carrying out the integration, giving

$$K^{eff} = K_u^{mc} + 2B_1 e - \frac{\mu_0 M_s^{\ 2}}{2} + \frac{K^s}{d} = K^v + \frac{K^s}{d} \qquad (1\text{-}11)$$

The volume anisotropy tern contains the magnetocrystalline anisotropy K_u^{mc}, a magnetostatic term $-\mu_0 M_s^{\,2}/2$, and magnetoelastic terms $2B_1 e$ arising from strains that are uniform throughout the film. The surface anisotropy term in Eq. (1-11) may arise from spin-orbital contributions or from strains that are localized at the surface. In a phenomenological sense, a magnetic contribution to the surface free energy of the crystal depends on the magnetization direction in the surface. The schematic diagram of practical magnetic anisotropies is shown in the following Fig. 1-7. The anisotropy energy E can be interpreted as with neglecting high order terms

$$E = K_{eff} \sin^2 \theta \tag{1-12}$$

Thus, when $\mathrm{K}^{\mathrm{eff}} > 0$, perpendicular (*out-of-plane*) magnetization is favored in the corresponding system; otherwise, the *in-plane* magnetization is favored when $\mathrm{K}^{\mathrm{eff}} < 0$.

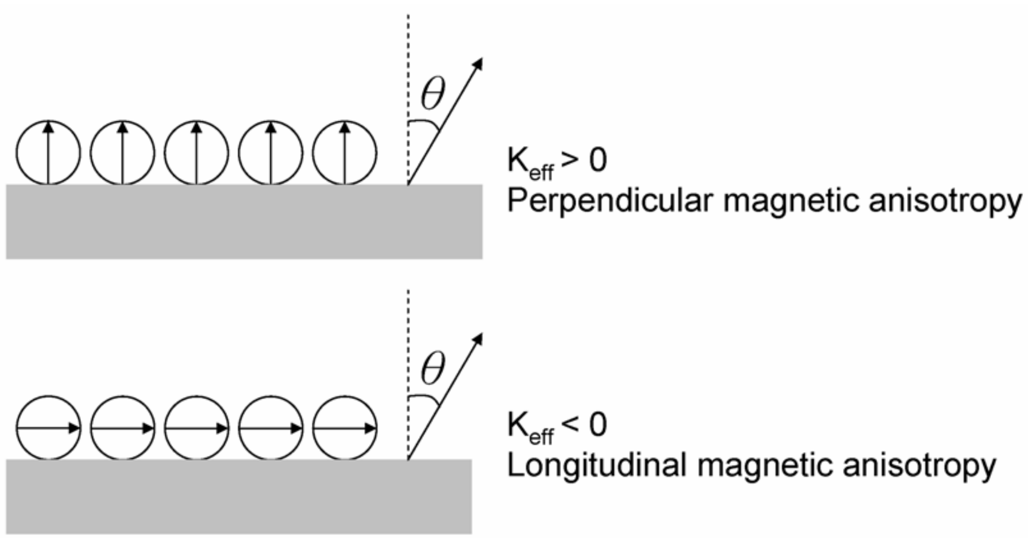

Fig. 1-7 Scheme of the surface magnetic anisotropies for perpendicular and longitudinal directions.

Part III Specific Pt-metal alloy surfaces:

For industrial purposes, Pt-M alloys (M: metal) are used in the form of small particles deposited on a substrate, and catalytic reactions for these alloy phases have generally been studied on aggregates.[21] Gauthier considered that although Pt may be combined with many other chemical elements, detailed and extensive experimental studies were conducted for a limited series of alloys: they concern 3D transition metals such as Fe, Co, Ni, and to a lesser extent Rh. All four species have atomic radii much smaller than Pt. Conversely, Sn has a size almost equal to that of platinum whereas Ti is much bigger. Such differences are worth noting since size effects are known to play a predominant role in the segregation process which occurs in the near surface region of bimetallic compounds. In other words, the atomic radii influence the composition and structure of the top layers that modified electronic distributions, the catalytic or chemical properties.

The crystallographic orientation of the surface can have a strong effect on the segregation. The (111) surfaces of Pt–Ni and Pt–Co alloys are enriched with platinum. PtCo and PtNi have very similar phase diagrams with a fcc disordered phase at high temperature.[22] At low temperature, ordered phases exist with the $L1_2$ structure around Pt_3M and PtM_3. The alloy has a tetragonal $L1_0$ structure around the equimolar composition of PtM.

1-7 Ni-Pt (nickel-platinum) alloys

Ni_xPt_{1-x} alloys have a face centered cubic (FCC) structure for all Ni concentration and are continuously soluble. Long-range chemical order develops at lower temperatures. Ni_xPt_{1-x} near the NiPt composition below 650ºC exhibits Cu-Au type ($L1_0$) phase.[23] Below 550ºC near the Ni_3Pt composition and below 510ºC near the $NiPt_3$ composition, Ni_xPt_{1-x} exhibits Cu_3Au type ($L1_2$) phase. The $L1_0$ phase has a tetragonal distortion, but the $L1_2$ phase has cubic symmetry. Like Co-Pt, Ni_xPt_{1-x} alloys are known to exhibit surface segregation in equilibrium. For the (100) and (111) orientation, the top layer of NiPt is enhanced to between 75% and 90% Pt, while the second layer is depleted of Pt. However, the (110) orientation has the reverse segregation, with the top layer being Ni-rich and the second layer being Pt-rich.[24] The measurements of low-energy electron diffraction (LEED) and ion scattering spectroscopy (ISS) also show a Pt enrichment at elevated temperatures for the (111) surface but a reverse behavior for $Pt_xNi_{1-x}(110)$ investigated by LEED: the surface layer was found to be enriched with Ni.[25] In general, intermetallic compounds that have magnetic ordering temperatures above room temperature are generally based on

3-d elements. However, the compounding of Ni with other elements generally results in a strong decrease of the Ni moment and a lowering of the Curie temperature to below room temperature. The Ni-Pt alloy system is indeed in many ways analogous to Co-Pt, but with significantly reduced Curie temperatures. In the following, the common binary compounds are listed in more detail.

I. Ni_3Pt compound

For Ni_3Pt, both the A1 (distorted fcc stacking) and $L1_2$ (Cu_3Au) phases are cubic, hence PMA must be a consequence of local ordering, caused by the growth process.[26] The PMA is appreciable even at room temperature, increase at lower temperature, and is much larger in (111)-oriented films than in (100) films. An A1 phase of Ni_3Pt has a Curie temperature of 115ºC while the $L1_2$ phase has a Curie temperature of 20ºC.[27] Perpendicular magnetic anisotropy was found in the (111) films of which have large clustering grown near 400ºC.

II. NiPt compound

NiPt is known to magnetically order at 115 K in the distorted fcc phase, but is paramagnetic in the completely $L1_0$ ordered phase. NiPt films grown between 200ºC and 400ºC show significant clustering. For the composition x ~47% of Ni_xPt_{1-x} in fcc phase the T_C is about 80 K. For the composition x ~50% Ni has fcc T_C about 115 K.[26] An (111) sample grown at 400ºC with slightly more Ni ($Ni_{52}Pt_{48}$) has PMA with K_u=2.5×10^6 erg/cm^3 measured at 150 K; however, after annealing, it becomes non-magnetic at 150 K.

III. $NiPt_3$ compound

$NiPt_3$ shows no sign of anisotropy and is not magnetically ordered in any known bulk equilibrium phase.[27] It is nonmagnetic in both the A1 and $L1_2$ bulk phases. More precisely, $NiPt_3$ is paramagnetic in the A1 phase, with a very small moment per Ni atom (~0.14μ_B) and nearly certainly nonmagnetic in the $L1_2$ phase due to the increased Ni-Ni separation. Nevertheless, Vasumathi et al.[26] found that (111) and (100) oriented $NiPt_3$ films grown at 350ºC show measurable magnetization with an onset at ~80 K and a broad magnetic transition. They considered the observation is indicative of significant Ni clustering. The magnitude of the moment of Ni is very susceptible to environmental effect. Generally, Ni must have at least three Ni neighbors to possess a moment and does not magnetically order, otherwise, the $L1_2$ long-range order is non-magnetic. In other words, clustering of Ni could produce the magnetization that can be measurable.

1-8 Co–Pt (cobalt-platinum) alloys

In equilibrium, Co_xPt_{1-x} alloys are known to show nearly complete surface segregation. Both the (111) and (100) surfaces are terminated with a pure Pt layer with significant Co enrichment of the second layer. For the (110) surface has just the reverse segregation, with the surface layer being Co rich and the second layer being Pt rich. In general, cobalt and platinum can form known ordered bulk alloys like Co_3Pt, CoPt and $CoPt_3$ compound.

I. Co_3Pt compound

The Co_3Pt alloy films possess hcp ordered phase, which consist of alternatively a Co layer, whereas the other consists of a $Co_{50}Pt_{50}$ layer.[28] The ordering of Co_3Pt alloy films can be induced by surface diffusion. The magnetic properties of Co_3Pt alloy films show a large energy-dependent perpendicular magnetic anisotropy (PMA).[29] The large magnetocrystalline anisotropy of ordered Co_3Pt ordered alloys has been shown to be attributed to the large spin-orbit coupling of the Pt atoms and a strong hybridization of the Pt d-bands with highly polarized Co d-bands.[30]

On the other hand, the hcp→fcc structural phase transition in bulk Co-Pt occurs by collective motions of large groups of atoms.[31] A transformation temperature between fcc→hcp and hcp→fcc transition temperatures is the equilibrium temperature which is relevant to MBE deposition since films are constructed atom by atom directly into their most stable crystal phase. As a result the transition temperature in Co_3Pt was discovered about 650 K.[32]

II. CoPt compound

Co_xPt_{1-x} alloys that can be used as permanent-magnet materials are found around the equiatomic composition for which the disordered fcc phase transform into an ordered face-centered-tetragonal (fct) phase.[33] This fct phase has a sufficient high uniaxial magnetic anisotropy, whereas the easy-magnetization direction being along the tetragonal c axis. The Curie temperature of CoPt is around 500ºC for the equiatomic composition and slightly decreases with increasing Pt concentration. The magnetic properties of $Co_{50}Pt_{50}$ nanoparticles did not show any coercivity in their as-grown state at room temperature.[34] However, at very low temperature about 5 K, coercivity of about 40 Oe was observed in the $Co_{50}Pt_{50}$ nanoparticles, which implies the superparamagnetic characteristics of the as-grown nanoparticles at room temperature. Studies of Co monolayers deposited on a (111) Pt surface show that a stable, two-monolayer-thick, fcc(chemically disordered) alloy forms after annealing at 375ºC.[35]

III. $CoPt_3$ compound

For thick $CoPt_3$ alloys, they were found that both the (111) and (100) orientations show a maximum of a perpendicular magnetic anisotropy around 400ºC.[36] The existence of a growth temperature around 690 K maximizing perpendicular anisotropy in (111) $CoPt_3$ films would be the result of conjugated strong surface diffusion.[37] Such a microstructure produces the observed distorted fcc stacking and would promote an axis of easy magnetization perpendicular to the film plane. A dominant surface diffusion process coupled with Pt segregation along the advancing surface during growth can thus yield the formation of (111) alternate Pt-rich and Pt-poor planar local regions. In contrast, the formation of the equilibrium $L1_2$–type structure in the film grown at 800 K is favored by a noticeable increase of volume mobility.

1-9 Ag-Pt (silver-platinum) alloys

In the solid Ag-Pt bulk alloy, chemically ordered phases do exist. The bulk enthalpy of mixing of the liquid Ag-Pt solution might thus compare better to the case of the disordered Ag-Pt(111) surface alloy, which is composed of clusters of one material randomly embedded in a matrix layer of the other component.[38] The solid solution of Ag-Pt possesses a large degree of immiscibility. No intermetallic phases were included due to controversy over their existence. Silver deposition on Pt(111) at or after annealing to temperatures above 600 K and below 900 K leads to a two-phase mixture for coverage ≤ 1 ML.[39] The authors found that the mixing is confined to the first layer and proceeds from the step edges. Annealing of the Ag/Pt(111) surface results in stress release within the Ag patches. Larger Ag islands dissolve into smaller 2D Ag clusters incorporated within the topmost Pt(111) layer or smaller 2D Pt clusters within the topmost Ag layer. The results are consistent with the AES and LEED studies that a disordered 2D Ag-Pt surface alloy is formed in the submonolayer range at 600-700 K.[40]